

Capillary evaporation on micromembrane-enhanced microchannel wicks with atomic layer deposited silica

Xianming Dai, Mehdi Famouri, Aziz I. Abdulagatov, Ronggui Yang, Yung-Cheng Lee, Steven M. George, and Chen Li

Citation: *Applied Physics Letters* **103**, 151602 (2013); doi: 10.1063/1.4824439

View online: <http://dx.doi.org/10.1063/1.4824439>

View Table of Contents: <http://scitation.aip.org/content/aip/journal/apl/103/15?ver=pdfcov>

Published by the AIP Publishing

Articles you may be interested in

[Modeling precursor diffusion and reaction of atomic layer deposition in porous structures](#)

J. Vac. Sci. Technol. A **33**, 01A104 (2015); 10.1116/1.4892385

[Biphilic nanoporous surfaces enabled exceptional drag reduction and capillary evaporation enhancement](#)

Appl. Phys. Lett. **105**, 191611 (2014); 10.1063/1.4901962

[Vacuum sealing using atomic layer deposition of Al₂O₃ at 250 °C](#)

J. Vac. Sci. Technol. A **32**, 01A101 (2014); 10.1116/1.4820240

[Mechanisms for hydrophilic/hydrophobic wetting transitions on cellulose cotton fibers coated using Al₂O₃ atomic layer deposition](#)

J. Vac. Sci. Technol. A **30**, 01A163 (2012); 10.1116/1.3671942

[Atomic layer deposition of ZnO/Al₂O₃/ZrO₂ nanolaminates for improved thermal and wear resistance in carbon-carbon composites](#)

J. Vac. Sci. Technol. A **30**, 01A149 (2012); 10.1116/1.3669518

The advertisement features a row of tablet computers displaying the cover of the journal 'Computing in Science & Engineering'. The covers show a colorful, abstract pattern. The text 'AIP's JOURNAL OF COMPUTATIONAL TOOLS AND METHODS. AVAILABLE AT MOST LIBRARIES.' is overlaid on the bottom right of the image. The 'computing in SCIENCE & ENGINEERING' logo is also present in the bottom right corner of the image area.

computing
in SCIENCE & ENGINEERING

AIP's JOURNAL OF COMPUTATIONAL TOOLS AND METHODS.
AVAILABLE AT MOST LIBRARIES.

Capillary evaporation on micromembrane-enhanced microchannel wicks with atomic layer deposited silica

Xianming Dai,¹ Mehdi Famouri,¹ Aziz I. Abdulagatov,² Ronggui Yang,³ Yung-Cheng Lee,³ Steven M. George,^{2,3} and Chen Li^{1,a)}

¹Department of Mechanical Engineering, University of South Carolina, Columbia, South Carolina 29208, USA

²Department of Chemistry and Biochemistry, University of Colorado, Boulder, Colorado 80309, USA

³Department of Mechanical Engineering, University of Colorado, Boulder, Colorado 80309, USA

(Received 11 July 2013; accepted 19 September 2013; published online 8 October 2013)

Due to the difficulty in depositing conformal coatings on high aspect ratio surfaces, capillary evaporation on superhydrophilic porous structures have not been well studied. In this work, superhydrophilic hybrid wick was fabricated by coating micromembrane-enhanced microchannels with 20 nm-thick silica (SiO_2) using the atomic layer deposited (ALD) technique. Rapid ALD SiO_2 coatings improve thin film evaporation of water on hybrid wicks by up to 56%. An appreciable enhancement of critical heat flux was not obtained in this study because of a compromise between the increased capillary pressure and viscous drag resulting from superhydrophilic ALD SiO_2 coatings. © 2013 AIP Publishing LLC. [<http://dx.doi.org/10.1063/1.4824439>]

Guided by the Wenzel's effect,¹ the apparent contact angle can be dramatically reduced via increasing the roughness of a hydrophilic surface. As a result, engineered surfaces with microscale,² nanoscale,³ and hierarchical⁴ structures were developed to enhance boiling and evaporation. However, it is challenging to distinguish the effect of augmented surface roughness and the effect of intrinsic wettability on heat transfer. Takata *et al.*⁵ investigated the effect of surface wettability on boiling and evaporation heat transfer using a sputtered titanium dioxide (TiO_2) thin layer on plain surfaces and enhanced heat transfer coefficient (HTC) and critical heat flux (CHF). Nonetheless, the sputtering method introduced additional surface roughness and superhydrophilicity of TiO_2 maintained by ultraviolet (UV) light. Most recently, Feng *et al.*⁶ reported approximately 200% CHF enhancement of pool boiling using atomic layer deposited (ALD) alumina (Al_2O_3) coatings. In previous studies, CHF was significantly enhanced on the flat surfaces,^{5,6} i.e., plain copper or Pt wires. Due to the difficulty in depositing conformal coatings on high aspect ratio surfaces, studies in evaporation on superhydrophilic surfaces are lacking. In this study, capillary evaporation on ALD SiO_2 coatings was studied. The enhanced capillary evaporation is critical to enhance performance of two-phase devices such as heat pipes that are widely used in electronic cooling, energy production, and recovery.⁷

ALD SiO_2 thin film coatings were selected because of its superior hydrophilic properties and chemical stabilities in water.^{8,9} The hydrophilicity of ALD SiO_2 coatings results from the high affinity silanol (Si-OH) groups on the surface.^{8,10,11} Compared to metal-organic chemical vapor deposition (MOCVD),¹² plasma enhanced chemical vapor deposition (PECVD),¹² radio frequency (RF) magnetron sputtering⁵ and solution based techniques,¹³ ALD technique has a unique capability to deposit highly conformal nanometer thick coatings on high aspect-ratio structures.¹⁴ The ALD

SiO_2 coatings can induce superhydrophilicity with surface roughness changing in an order of 10 nm or less. Equally important, because of the sequential self-terminating gas-solid reactions, ALD techniques can achieve strong bonding between coatings and their substrates.¹⁰ Additionally, surface morphology and chemical property controls are essential for long term operations in industrial applications.¹⁵ ALD coatings can serve as corrosion protection layers of heat transfer surfaces¹⁶ because copper corrosion and dissolution often imposes limitations on the long-term performance of heat exchangers.^{15,17}

To enhance capillary evaporation, a type of micromembrane-enhanced microchannel wicks consisting of a single-layer copper woven meshes and a microchannel array were developed as shown in Fig. 1.¹⁸ The copper woven mesh (mesh number: 1509 m^{-2} and wire diameter: $56\ \mu\text{m}$) was attached on the microchannels by a diffusion bonding technique to minimize thermal contact resistance.¹⁹ The evaporation surfaces were sintered on a $1 \times 1\text{ cm}^2$ squared copper block and coated SiO_2 using ALD. During tests, evaporation surfaces were positioned in the vertical direction and with an approximately 15 mm distance from the center of a heating area to the water level to minimize the impacts of pool boiling.¹⁸

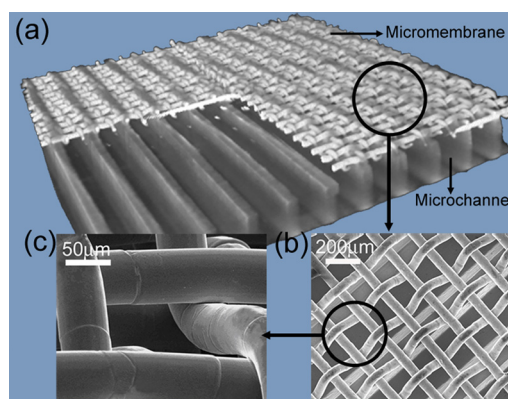


FIG. 1. Structure of the micromembrane-enhanced microchannel wicks developed in Ref. 18.

^{a)}Author to whom correspondence should be addressed. Electronic mail: Li01@mailbox.sc.edu.

ALD was carried out at 150 °C in a viscous-flow hot-wall type ALD reactor.²⁰ Prior to SiO₂ deposition, Al₂O₃ was pre-deposited as a seed layer to facilitate SiO₂ nucleation and growth to ensure conformality of ALD SiO₂ coatings. The number of ALD Al₂O₃ deposition cycles was approximately 80 at a typical growth rate of 0.1 nm/cycle. After 80 cycles of Al₂O₃ coatings, one cycle of Rapid ALD SiO₂ was applied at an approximate growth rate of 12 nm/cycle. The total thickness of the ALD Al₂O₃ and SiO₂ coatings was approximately 20 nm, while the thicknesses of ALD Al₂O₃ and ALD SiO₂ films are 8 nm and 12 nm, respectively. Bare hybrid wicks were cleaned using oxygen plasma for 60 s to create hydrophilic copper oxide (CuO) coatings²¹ as a reference sample.

Figure 2 shows the morphologies of the ALD SiO₂-coated surface that was characterized using atomic force microscopy (AFM). The Root Mean Square (RMS) roughness, R_q , is used to characterize the surface roughness.

$$R_q = \sqrt{\frac{1}{MN} \sum_{i=1}^M \sum_{j=1}^N (Z_{ij} - Z)^2}, \text{ where } R_q \text{ is the RMS roughness; } M, N \text{ are the total sampling times in the length and width direction; } i, j \text{ are the sampling times; } Z_{ij} \text{ is the sampling height; and } Z \text{ is the average height.}$$

The RMS roughness on a plain copper surface is 1.2 nm and increased to 2.9 nm after the ALD coating. This indicates that the change of surface roughness resulting from ALD SiO₂ coatings is minor; and that the impact of surface area augmentation on heat transfer can be ignored. As shown in Figs. 2(a) and 2(b), a three dimensional (3D) AFM images well illustrated the conformality of the ALD SiO₂ coating.

The static contact angle was measured with a 5 μ l highly purified water droplet. Before the measurement, samples were cleaned by plasma for 15 s with an oxygen flow rate of 6 ml/min to remove carbon contaminations. The water contact angle on the plain surface was reduced from 49.6° (Fig. 2(c)) to 4.7° (Fig. 2(d)) using ALD SiO₂ coating, i.e., more hydrophilic. The apparent contact angle on the ALD SiO₂-coated hybrid wicking structure was measured to be nearly 0° because of the Wenzel's effect (Fig. 2(e)).¹

Capillary evaporation on three types of micromembrane-enhanced microchannel wicks, i.e., bare, ALD SiO₂ coated,

and oxygen plasma-treated surfaces were experimentally evaluated. Compared to hybrid wicks without ALD coatings, as shown in Figs. 3(a) and 3(b), CHF is not enhanced using ALD SiO₂. However, HTC is significantly improved using ALD SiO₂ coatings, for example, from 9.1 W/(cm²K) to 14.2 W/(cm²K) at a heat flux of 139.3 W/cm², representing a 56% enhancement (Fig. 3(a)). However, CuO created by oxygen plasma cannot sustain since enhancement was not observed in the higher heat flux (Fig. 3(a)). A repeat test on ALD coatings further confirmed the HTC enhancement as shown in Fig. 3(a). The results demonstrated that HTC is primarily enhanced by ALD SiO₂ coatings, not the plasma induced CuO.

The evaporation process on the bare micromembrane-enhanced microchannel wicks can be divided into three regions¹⁸ (Fig. 3(b)). In this study, to further reveal heat transfer mechanisms in these three regions, a two-dimensional (2D) heat conduction model was developed to simulate temperature distribution in the cross section in three regions as shown in Figs. 3(c)–3(f).²² In region I, nucleate boiling is primarily initiated on the bottom walls of microchannels because the sufficient superheat (i.e., 100.86 °C as shown in Fig. 3(d)). In region II, the temperature on side walls reached 104.8 °C (Fig. 3(e)), high enough to trigger nucleate boiling. However, the heat transfer is still dominated by thin film evaporation on micromeshes since the required superheat to initiate nucleate bubbles on the micromembrane (with relatively smaller cavities) is higher than that on microchannels as guided by Hsu's model (Fig. 3(e)).²³ In region III, the temperature on meshes reached 109.4 °C (Fig. 3(f)) and the liquid supply is sufficient after the oscillating flows resumed.¹⁸ As a result, the nucleate boiling can occur simultaneously inside the microchannels and on micromembrane,²⁴ as confirmed by the visualization study.

As shown in Fig. 3(b), in region I, the shape of evaporation curves is similar on the bare and ALD SiO₂ coated hybrid wicks, but HTC is considerably enhanced by ALD coatings. Visualization study shows that the ALD SiO₂ coated hybrid wicks appear to be fully saturated with liquid (Figs. 4(a) and 4(e)), however, the bare micromembrane was not. This is further explained in Figs. 4(i)–4(l). The static wetting height in microchannels is described as: $h = (2\gamma\cos\theta)/(\rho gR)$, where h is

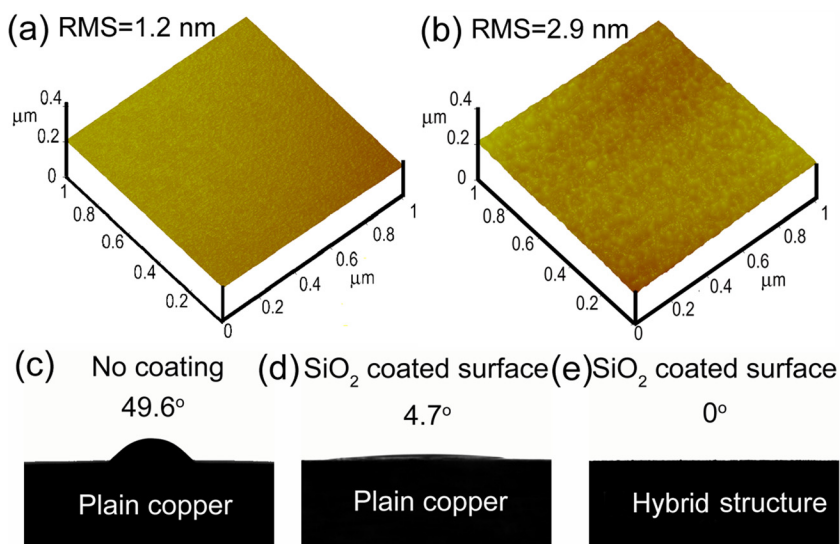


FIG. 2. Characterization of ALD SiO₂ coatings. (a) A three dimensional (3-D) AFM image of bare copper mesh. (b) A 3-D AFM image of the conformal SiO₂ ALD coated copper mesh. (c) Contact angle on bare copper sheet. (d) Contact angle on ALD coated copper sheet. (e) Contact angle on ALD coated hybrid structure.

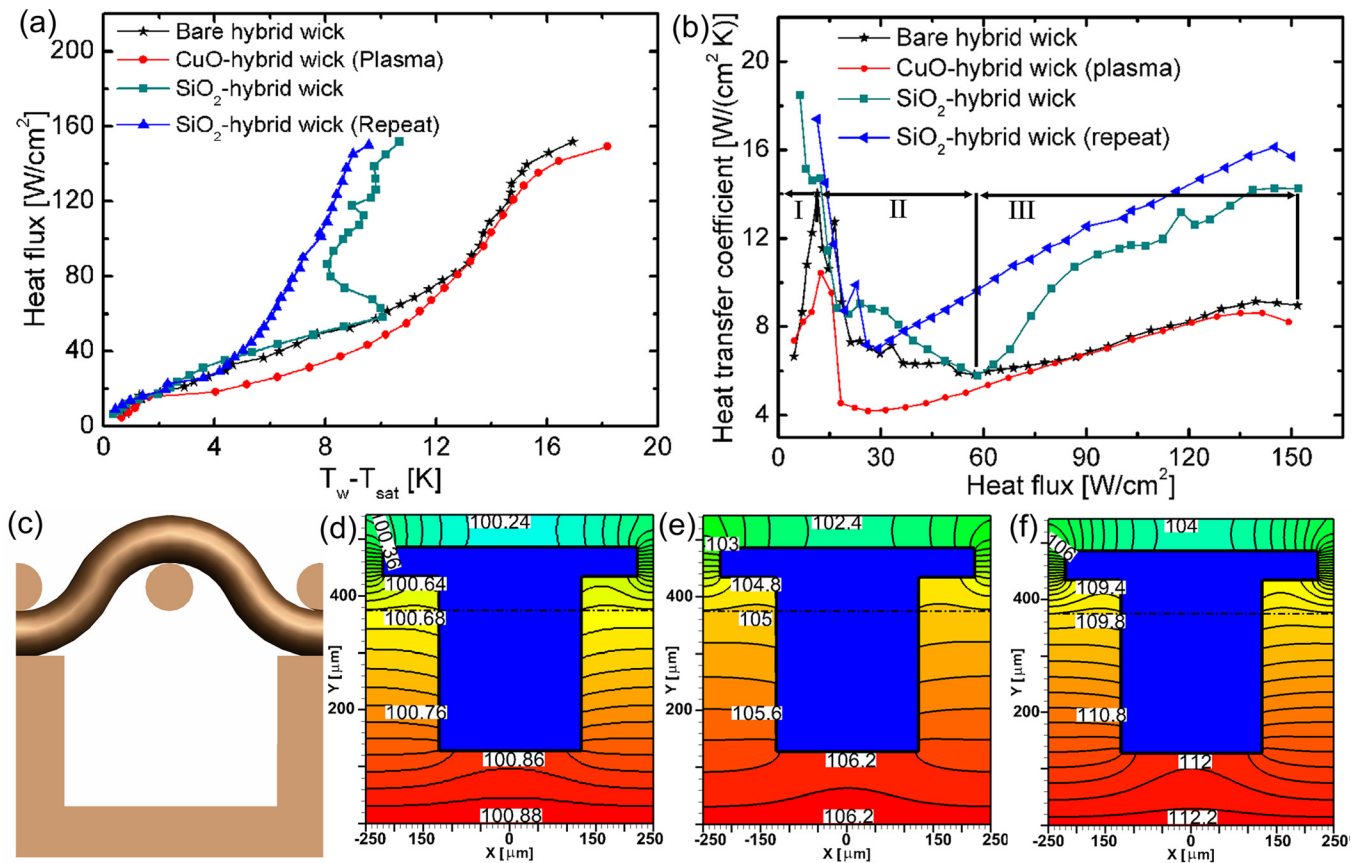


FIG. 3. Capillary evaporation heat transfer curves on micromembrane-enhanced microchannel wicks with various surface treatments. (a) ΔT - q'' curves. (b) q'' - h curves. (c) Schematic view of the wick. (d) Temperature distribution at a heat flux of 9.0 W/cm² in region I. (e) Temperature distribution at a heat flux of 40.4 W/cm² in region II. (f) Temperature distribution at a heat flux of 61.4 W/cm² in region III. The unit of temperature is °C for (d), (e), and (f).

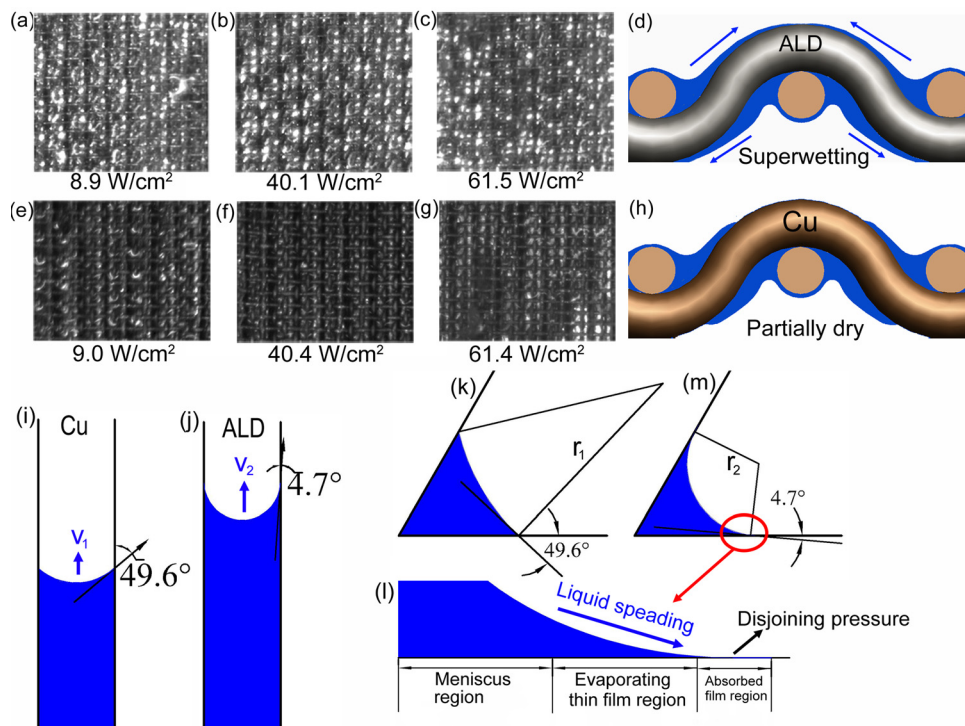


FIG. 4. The superhydrophilic property enabled by ALD SiO₂ coatings. (a)–(c) Liquid distributions on the ALD SiO₂-coated structures at heat fluxes of 8.9, 40.1 and 61.5 W/cm² (enhanced online) [URL: <http://dx.doi.org/10.1063/1.4824439.1>] [URL: <http://dx.doi.org/10.1063/1.4824439.2>] [URL: <http://dx.doi.org/10.1063/1.4824439.3>]. (d) Schematic diagrams of liquid distribution on the ALD SiO₂ coated wicks. (e)–(g) Liquid distribution on the bare wicks at heat fluxes of 9.0, 40.4 and 61.4 W/cm² (enhanced online) [URL: <http://dx.doi.org/10.1063/1.4824439.4>] [URL: <http://dx.doi.org/10.1063/1.4824439.5>] [URL: <http://dx.doi.org/10.1063/1.4824439.6>]. (h) Schematic diagrams of liquid distributions on the bare wicks. (i) Capillarity in a bare Cu tube. (j) Capillarity in an ALD SiO₂ coated tube. (k) Cross-section of meniscus on a bare copper corner. (l) Liquid film distribution on ALD SiO₂ coated interfaces. (m) Cross-section of meniscus on an ALD SiO₂ coated corner.

the static capillary length; γ is the surface tension of water; θ is the contact angle; ρ is liquid density; and R is the half width of the microchannel. Since the contact angle was reduced from 49.6° to 4.7° , h_2 should be larger than h_1 (Figs. 4(i) and 4(j)). As a result, the HTC on ALD SiO₂-coated hybrid wicks is significantly enhanced in the low heat flux region I. Furthermore, liquid wetting and rewetting occur on the micro-meshes and the wetting frequency increases with the increasing heat flux (Fig. 5(a)), resulting in strong advection, which agrees with the multilayer liquid wetting model.²⁵

Region II is a transition region¹⁸ where the liquid oscillations were temporarily suspended. In this region, bubbles start to nucleate on the microchannel sidewalls because of sufficiently high superheat established on the sidewall (Fig. 3(e)). The substantially enhanced nucleate boiling eventually leads to global liquid supply crisis and hence the formation of vapor cores inside microchannels.¹⁸ As a result, the capillary flows are suspended in region II.²² The heat transfer in region II is dominated by thin film evaporation inside microchannels and on the micromeshes. The average HTC on ALD SiO₂ coated surfaces in region II is approximately 15% higher than that on the bare ones because of the improved wetting, i.e., fully wetted ALD SiO₂ coatings (Fig. 4(b)) at a heat flux of 40.4 W/cm^2 (Fig. 4(f)).

In region III, nucleate boiling and capillary evaporation are established on copper meshes because of the high superheat

(Fig. 3(f)), which induces menisci receding and rewetting processes in sharp corners and oscillating flows. Therefore, instead of from microchannels, higher capillary force is generated from micromembrane (with significantly smaller meniscus radii.) to sustain liquid supply under high heat flux conditions. In region III, liquid supply and fluid oscillations are resumed. As a result, the thin film evaporation on ALD coatings is substantially enhanced (Fig. 3(b)). The superhydrophilic ALD SiO₂ coatings greatly enhance the local wetting and rewetting processes (Figs. 4(d) and 4(m)) and hence sustain and greatly extend thin liquid film under high heat flux conditions (Figs. 4(c) and 4(g)). As shown in Figs. 4(d) and 4(h), partial dryout or "hot spot" occurred on bare meshes was not observed on the ALD SiO₂ coated meshes (Fig. 4(m)). According to the Washburn's law,²⁶ for a given time the penetrated wetting distance, L , increases with the reduced contact angle, as described in $L = (R\sigma\cos\theta/(2\mu))^{1/2} t^{1/2}$, where R is the half width of microchannels; σ is the liquid surface tension; θ is the contact angle; μ is the liquid dynamic viscosity; and t is the penetrating time. This also indicates the wetting velocity, v_2 , in a superhydrophilic microchannel is higher than that, v_1 , in a bare microchannel. Thus, wetting areas substantially increase and can be sustained by superhydrophilic ALD SiO₂ coatings (Figs. 4(a)–4(c)) during evaporation. In addition, the local liquid distributions are improved by the ALD SiO₂ coatings (Figs. 4(k)

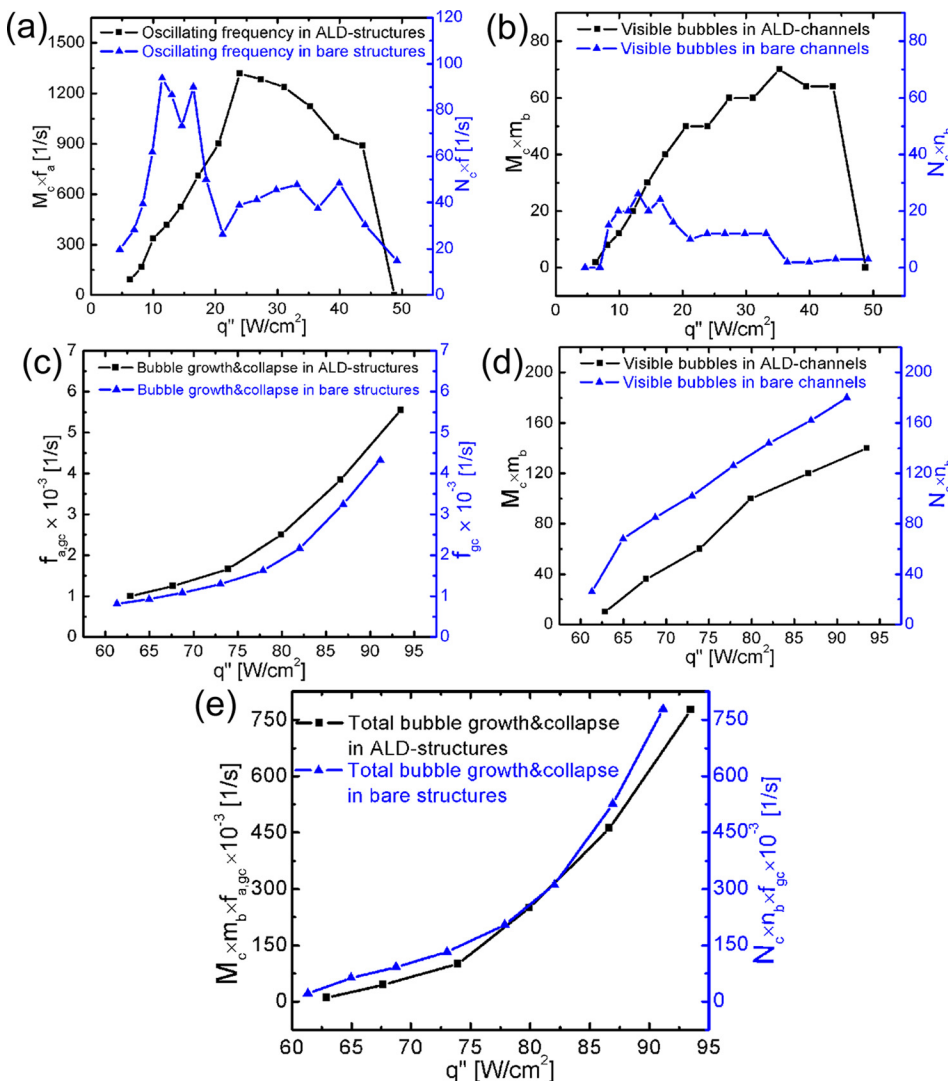


FIG. 5. Comparisons of oscillating flows on the ALD SiO₂ coated and bare wicks. (a) The total oscillating frequency, $M_c \times f_a$, on the ALD SiO₂ coated micromembrane-enhanced microchannel wicks; M_c is the number of active channels; and f_a is the frequency of fluid flow in a single active channel. $N_c \times f$ is for the bare structure. (b) The total number of visible bubbles in active channels, $M_c \times m_b$. M_c is the number of visible bubbles in a single active channel; and m_b is the number of active channels. $N_c \times n_b$ is for the bare structure. (c) Bubble growth and collapse frequency, $f_{a,gc} \times f_{gc}$ is for the bare structure. (d) The total number of visible bubbles in active channels, $M_c \times m_b$, in the high heat flux region. $N_c \times n_b$ is for the bare structure. (e) Total bubble growth and collapse frequency, $M_c \times m_b \times f_{a,gc}$ is for ALD coated structure, $N_c \times n_b \times f_{gc}$ is for the bare structure.

and 4(m)) since the superhydrophilic interface yields a smaller film pressure gradient and larger friction drag,²⁷ resulting in a thinner liquid film during evaporating. Thus, the local thin film evaporation is enhanced by improving wettability.²⁸

Figure 5(a) shows that the frequency of oscillating flows on the ALD SiO₂ coated evaporating surfaces is approximately one order of magnitude greater than that of the bare structures in the low heat flux region. The number of visible bubbles in the low heat flux region also increases significantly because of the ALD SiO₂ coating (Fig. 4(b)). The increased frequency of bubble growth and collapse (Fig. 4(c)) can be caused by a high bubble growth rate resulting from the enhanced thin film evaporation in the microlayer.²⁹ Note that the bubble dynamics are different from those in pool boiling because of the absence of buoyancy force.²⁹ The number of visible bubbles on the ALD SiO₂ coatings is reduced (Fig. 5(d)) since some of the superhydrophilic cavities could become inactive as a result of flooding.^{24,30} The total bubble growth and collapse frequency are nearly identical on the bare and ALD coated evaporating surfaces (Fig. 5(e)), strongly implying that the HTC enhancement primarily resulted from the improved thin film evaporation and advection, instead of the enhanced nucleate boiling.

In the above, we articulated the enhanced HTC on ALD SiO₂-coated hybrid wicks results from the improved local wetting that substantially enhances thin film evaporation and advection. However, CHF of capillary evaporation is not significantly enhanced by the ALD SiO₂ coatings. CHF is determined by the global liquid supply, specifically, by the capillary pressure generated by micromeshes and the flow resistance in microchannels. When evaporation approaches the CHF condition, thin film evaporation occurs primarily on micromembrane and the liquid film is maintained by disjoining pressure. The major pressures that determine fluid flows are capillary pressure (Δp) and viscous drag ($\Delta p'$). The former is determined by Young-Laplace equation: $\Delta p = 2\sigma/r$, where Δp is capillary pressure, σ is surface tension and r is the principal radius of curvature. The reduced contact angle results in a reduced meniscus in a conformal sharp corner,²⁸ that is, $r_1 < r_2$ (Figs. 4(k) and 4(m)), where r_1 and r_2 are the radii of curvature for bare and ALD SiO₂ coated structures. Herein, higher capillary pressure can be generated on ALD SiO₂ coatings than that on the bare surfaces. However, superhydrophilic coatings also result in higher viscous drag.³¹ In addition, the increased fluid velocity in the microchannels would result in higher flow resistance on the superhydrophilic surfaces as indicated by the pressure drop in microchannels: $\Delta p' = 1/2 f \rho v^2 L_0 / D_h$, where $\Delta p'$ is the pressure drop through the channel; v is the fluid velocity; L_0 is the flow length; D_h is the hydrodynamic diameter; and f is the friction factor. As a result, the increased capillary force from ALD SiO₂ coatings could be compromised by the high viscous drag.

In summary, we demonstrated that conformal superhydrophilic ALD SiO₂ coatings can significantly enhance capillary evaporation because of the improved wettings and the induced advection in the low heat flux region and the enhanced thin film evaporation in the high heat flux region. An appreciable enhanced CHF was not achieved as a result of the compromise between the increased capillary pressure and viscous drag resulting from superhydrophilic ALD SiO₂ coatings.

This work was supported by the Defense Advanced Research Projects Agency (DARPA) Thermal Ground Plane under Grant No. N66001-08-C-2006 and by the Office of Naval Research (Program Officer Dr. Mark Spector) under Grant No. N000141210724. The authors thank the electron microscopy center at the University of South Carolina for instrument use, scientific and technical assistance. Li-Anne Liew and Susan Song's help on ALD coatings, Yingchao Yang's help on AFM measurement of surface roughness and Dr. Xingjie Zan's help on the contact angle measurement are greatly appreciated.

¹R. N. Wenzel, *J. Phys. Chem.* **53**(9), 1466 (1949).

²C. Li, G. P. Peterson, and Y. X. Wang, *ASME Trans. J. Heat Transfer* **128**(12), 1312 (2006).

³C. Li, Z. K. Wang, P. I. Wang, Y. Peles, N. Koratkar, and G. P. Peterson, *Small* **4**(8), 1084 (2008).

⁴C. H. Li, T. Li, P. Hodgins, C. N. Hunter, A. A. Voevodin, J. G. Jones, and G. P. Peterson, *Int. J. Heat Mass Transfer* **54**(15–16), 3146 (2011); K. H. Chu, Y. S. Joung, R. Enright, C. R. Buie, and E. N. Wang, *Appl. Phys. Lett.* **102**, 151602 (2013).

⁵Y. Takata, S. Hidaka, J. M. Cao, T. Nakamura, H. Yamamoto, M. Masuda, and T. Ito, *Energy* **30**(2–4), 209 (2005).

⁶B. Feng, K. Weaver, and G. P. Peterson, *Appl. Phys. Lett.* **100**(5), 053120 (2012).

⁷M. Mochizuki, T. Nguyen, K. Mashiko, Y. Saito, T. Nguyen, and V. Wuttijumong, *Front. Heat Pipes* **2**, 013001 (2011).

⁸P. Vassallo, R. Kumar, and S. D'Amico, *Int. J. Heat Mass Transfer* **47**(2), 407 (2004).

⁹N. R. Jana, C. Earhart, and J. Y. Ying, *Chem. Mater.* **19**(21), 5074 (2007).

¹⁰P. K. Jal, S. Patel, and B. Mishra, *Talanta* **62**(5), 1005 (2004).

¹¹E. P. Ng and S. Mintova, *Microporous Mesoporous Mater.* **114**(1–3), 1 (2008).

¹²H. T. Phan, N. Caney, P. Marty, S. Colasson, and J. Gavillet, *C. R. Mec.* **337**(5), 251 (2009).

¹³W. Wu, H. Bostanci, L. C. Chow, Y. Hong, M. Su, and J. P. Kizito, *Int. J. Heat Mass Transfer* **53**(9–10), 1773 (2010).

¹⁴J. W. Elam, D. Routkevitch, P. P. Mardilovich, and S. M. George, *Chem. Mater.* **15**(18), 3507 (2003); S. M. George, *Chem. Rev.* **110**(1), 111 (2010).

¹⁵B. Kuznicka, *Eng. Failure Anal.* **16**(7), 2382 (2009).

¹⁶A. I. Abdulagatov, Y. Yan, J. R. Cooper, Y. Zhang, Z. M. Gibbs, A. S. Cavanagh, R. G. Yang, Y. C. Lee, and S. M. George, *ACS Appl. Mater. Interfaces* **3**(12), 4593 (2011).

¹⁷N. Boulay and M. Edwards, *Water Res.* **35**(3), 683 (2001).

¹⁸X. M. Dai, F. H. Yang, R. G. Yang, Y. C. Lee, and C. Li, *Int. J. Heat Mass Transfer* **64**(0), 1101 (2013).

¹⁹C. Li and G. P. Peterson, *Int. J. Heat Mass Transfer* **49**(21–22), 4095 (2006).

²⁰J. W. Elam, M. D. Groner, and S. M. George, *Rev. Sci. Instrum.* **73**(8), 2981 (2002).

²¹P. Luzeau, X. Z. Xu, M. Lagues, N. Hess, J. P. Contour, M. Nanot, F. Queyroux, M. Touzeau, and D. Pagnon, *J. Vac. Sci. Technol. A* **8**(6), 3938 (1990).

²²See supplementary material at <http://dx.doi.org/10.1063/1.4824439> for assumptions and boundary conditions of temperature profile simulations, experimental setup and procedure, data reduction, and multimedia files.

²³Y. Y. Hsu, *J. Heat Transfer* **84**, 207 (1962).

²⁴X. M. Dai, X. Y. Huang, F. H. Yang, X. D. Li, J. Sightler, Y. C. Yang, and C. Li, *Appl. Phys. Lett.* **102**(16), 161605 (2013).

²⁵R. Xiao, K. H. Chu, and E. N. Wang, *Appl. Phys. Lett.* **94**(19), 193104 (2009).

²⁶E. W. Washburn, *Phys. Rev.* **17**(3), 273 (1921); A. A. Darhuber, S. M. Troian, and W. W. Reisner, *Phys. Rev. E* **64**(3), 031603 (2001).

²⁷F. Heslot, A. M. Cazabat, P. Levinson, and N. Fraysse, *Phys. Rev. Lett.* **65**(5), 599 (1990).

²⁸A. J. Jiao, H. B. Ma, and J. K. Critser, *Int. J. Heat Mass Transfer* **50**(15–16), 2905 (2007).

²⁹Y. Nam, E. Aktinol, V. K. Dhir, and S. Ju, *Int. J. Heat Mass Transfer* **54**(7–8), 1572 (2011).

³⁰N. A. Patankar, *Soft Matter* **6**(8), 1613 (2010).

³¹H. Y. Wu and P. Cheng, *Int. J. Heat Mass Transfer* **46**(14), 2547 (2003).